Sensors and Actuators B 262 (2018) 70–78

Contents lists available at ScienceDirect

Sensors and Actuators B: Chemical

journal homepage: www.elsevier.com/locate/snb

Enhanced triethylamine sensing properties by fabricating Au@SnO_2/α-Fe_2O_3 core-shell nanoneedles directly on alumina tubes

Hongyan Xu [a], Wenru Li [a], Rui Han [a], Ting Zhai [a], Huanqin Yu [a], Zhengrun Chen [a], Xiangwen Wu [b], Jieqiang Wang [a], Bingqiang Cao [a,*]

[a] School of Materials Science and Engineering, University of Jinan, Jinan 250022, Shandong, P.R. China
[b] College of Chemistry, Chemical Engineering and Materials Science, Collaborative Innovation Center of Functionalized Probes for Chemical Imaging, Key Laboratory of Molecular and Nano Probes, Ministry of Education, Shandong Normal University, Jinan 250014, P.R. China

ARTICLE INFO

Article history:
Received 12 September 2017
Received in revised form 2 January 2018
Accepted 26 January 2018
Available online 31 January 2018

Keywords:
α-Fe_2O_3 nanoneendles
Direct growth method
Schottky contact
N–N heterojunction
TEA sensor

ABSTRACT

α-Fe_2O_3 nanoneedles were directly grown on the surface of Al_2O_3 tubes by a cost-effective hydrothermal method. In addition, the construction of Au nanoparticle-loaded SnO_2/α-Fe_2O_3 core/shell heterostructure was fabricated by employing pulsed laser deposition (PLD) and DC-sputtering methods Gas sensors were fabricated from Au@SnO_2/α-Fe_2O_3 core-shell nanoneedles on Al_2O_3 tubes, and their sensing properties have investigated for response to various target gases. The results indicated that the sensor based on Au@SnO_2/α-Fe_2O_3 core-shell nanoneedles showed superior selectivity toward triethylamine (TEA) gas, giving a response of 39–100 ppm, which was higher than that of α-Fe_2O_3 nanoneedles and SnO_2/α-Fe_2O_3 core-shell nanoneedles. Moreover, the sensor based on Au@SnO_2/α-Fe_2O_3 core-shell nanoneedles showed an obvious better linearity (R = 0.9975) of sensing characteristics than of two other sensors. The enhanced sensing properties are discussed with the semiconductor depletion layer model along with the Schottky contact and N–N heterojunction theory.

1. Introduction

Gas sensors have got a lot of attentions in many applications for a long time, including detecting toxic and flammable gases [1], biochemical detection [2], food quality control [3], and so on, which working based on the electrical variation caused by the chemical reaction between the electrons and various gases and vapors [4]. Among the various gases, triethylamine (TEA) is a kind of important gas which has a relationship to both food safety and human health. Because TEA can be secreted in dead fish and sea creatures and can result in serious damage to human health when the concentration is more than 10 ppm on volumetric basis (ppmV) in air, such as eye and skin chemical burns, headaches, and pulmonary edema [5–7]. Therefore, it is necessary to realize an accurate and fast detection of TEA with high sensitivity and good selectivity in biomedical, chemical, food industries and our daily life [5].

Various metal oxide semiconductors (MOSs) have been used into the field of gas sensors due to their superior stability, low cost and simple preparation [8–16]. Among these available types, Alpha-iron oxide (α-Fe_2O_3) has received much research attention due to its high resistance to corrosion, abundant raw material and non-toxicity [17]. As an n-type MOSs, Fe_2O_3 has a direct band gap (E_g) of 2.1 eV and is the most thermodynamically stable phase among all iron oxides under ambient conditions. Thus Fe_2O_3 has been extensively used for some fields, such as catalysts, wastewater treatment, pigment, magnetic material, electrode materials in lithium ion batteries, and gas sensors [18–23].

It is well known that the morphology and microstructure of the gas sensing material can affect the adsorption, diffusion, and interfacial reaction of the target molecules on its surface, which determine the gas-sensing response characteristics of the material [24,25]. Moreover, the particle size and morphology usually show a great effect on the gas- or vapor-sensing performance of semiconductor metal oxides [26–28]. And consequently, a lot of effort has been made on the controlling synthesis of various Fe_2O_3 nanostructures, including nanospindles [29], nanorods [30], nanowires [31], nanobelts [32], nanotubes [33], nanorings [34], and nanospheres [35]. On the other hand, the precious metals decorated on both oxide semiconductors and hetero-nanostructures consisted of two or more metal oxides can improve the sensing performance. The enhanced sensing mechanism can be explained by the Schottky

* Corresponding author at: Materials Research Center for Energy and Photoelectrochemical Conversion, School of Materials Science and Engineering, University of Jinan, Jinan 250022, P.R. China.
E-mail address: mse_caobq@ujn.edu.cn (B. Cao).

https://doi.org/10.1016/j.snb.2018.01.209
0925-4005/

contact or spillover effect of precious metals and the change of resistance caused by the formation of a hetero-junction [36]. The mainly effective methods to improve the gas properties of MOSs at present are summarized in the above two parts.

Inspired by these works, we design Au@SnO_2/α-Fe_2O_3 nanostructure to improve the TEA sensing performances of α-Fe_2O_3. Herein, we developed a one-step facile hydrothermal route to build the pristine α-Fe_2O_3 nanoneedles (FNs) directly on Al_2O_3 tubes. Furthermore, in order to improve the gas performance of α-Fe_2O_3 nanoneedles, we have a research from the point of building hetero-junction and Schottky contact. The SnO_2/α-Fe_2O_3 nanoneedles (SFNs) and Au@SnO_2/α-Fe_2O_3 nanoneedles (ASFNs) were composited on the basic of FNs by pulsed laser deposition and DC-sputtering process, respectively. As expected, the sensing properties of Au@SnO_2/α-Fe_2O_3 nanoneedles sensor are better than that of prinstine α-Fe_2O_3 nanoneedles sensor, which is 1.5 times higher in response and with an obvious better linearity (R = 0.9975) of sensing characteristics. The formations of Schottky contact and N–N heterojunction are the key factors to enhance sensing performances and the mechanisms are discussed in detail.

2. Experimental

2.1. Directly growth of FNs on Al_2O_3 tubes

All the chemical reagents were analytical graded and used without further purification. In the experiment, cleaned alumina (Al_2O_3) tubes ((4.0 mm in length, 1.0 mm in internal diameter and 1.4 mm in external diameter) with a pair of Au electrodes (2.0 mm in distance) attached with Pt lead wires) were immersed into a mixed aqueous solution of 0.5 mol/L of $FeCl_3$ and 0.1 mol/L of Na_2SO_4. And the mixture was transferred into a Teflon-lined stainless steel autoclave. The autoclave was heated to 140 °C for 12 h and then cooled to room temperature. After that, the Al_2O_3 tubes were taken out from the solution and washed for several times with deionized water and ethanol. After drying, the Al_2O_3 tubes were annealed 600 °C for 2 h.

2.2. Growth of SFNs and ASFNs

A shell of SnO_2 nanoparticles was deposited onto the surface of FNs by pulsed laser deposition (PLD) method using SnO_2 target at room temperature. The typical PLD growth condition for SnO_2 was as following: A KrF laser of 1 mJ/cm^2 and an oxygen partial pressure of 3×10^{-4} Pa were typically applied. The laser pulses were controlled for 1000 pules and SFNs heterojunctions were grown on Al_2O_3 substrates. After that, Au nanoparticles were loaded onto the SFNs by DC-sputtering with a working time of 30 s. The preparation flow-process diagram of sensor based on α-Fe_2O_3 nanosheets was shown in Fig. S1 in the Supplementary material.

2.3. Material characterizations and sensor properties

The morphology, microstructure, and composition of materials were measured by a field emission scanning electron microscope (FESEM, FEI QUANTA FEG250) equipped with energy dispersive X-ray spectroscopy (EDS, INCA MAX-50) and a high-resolution transmission electron microscope (HRTEM, JEM-2100F, JEOL) with energy dispersive X-ray spectroscopy (EDS, Oxford Link Isis). The phase of sensing materials was checked with X-ray diffraction (XRD, D8-Advance, Bruker). The surface elemental composition was checked with X-ray photoelectron spectroscopy (XPS, Thermo ESCALAB 250XI). Differential thermal analysis and thermogravimetry (TG/DTA, STA-409-EP, Netzsch) were conducted to study the oxidation progress of α-Fe_2O_3 powder under air from 25 to 800 °C with a heating rate of 10 °C/min. A gas-sensing test system (WS-30A, Weisheng Electronics, China) was used to test the gas sensing properties of the as-prepared sensors. During the test, the devices were put into an airproof test box. Target gases with calculated concentration were injected into the testing chamber by a microsyringe.

3. Results and discussion

3.1. Structural and morphological characteristics

First of all, the TG-DSC result is shown in Fig. 1(a). As can be clearly seen from the inset picture in Fig. 1(a), the color of the powder changes from yellow to orange after an annealing process. Analyzing the DSC curve, the weight loss of the samples undergoes three steps from room temperature to 800 °C. The sample has an apparently decrease in weight at about 90 and 240 °C (endothermic peaks) which corresponding to the removal of physically adsorbed water and chemically adsorbed water, respectively. At about 370 °C, there is a weak exothermic peak on the DTA curve. Correspondingly, there is no apparently change in the weight as illustrated by the TG curve. So it can be inferred that the samples transformed from γ-Fe_2O_3 to α-Fe_2O_3 according to the reference [37]. In order to further analyze the phase and crystal structure of the samples, the four kinds of samples were characterized by the XRD as shown in Fig. 1(b). The sample No.1 is unannealed powder which all diffraction peaks can be easily indexed to the α-FeOOH (JCPDS Card No. 29-0713). According to the result of TG-DSC, we annealed powder No. 1 at 600 °C for 2 h and obtained powder No.2. By comparing, the diffraction peaks of sample No.2 match well to the diffraction pattern of typical hexagonal Fe_2O_3 phase (JCPDS Card No. 89-596).

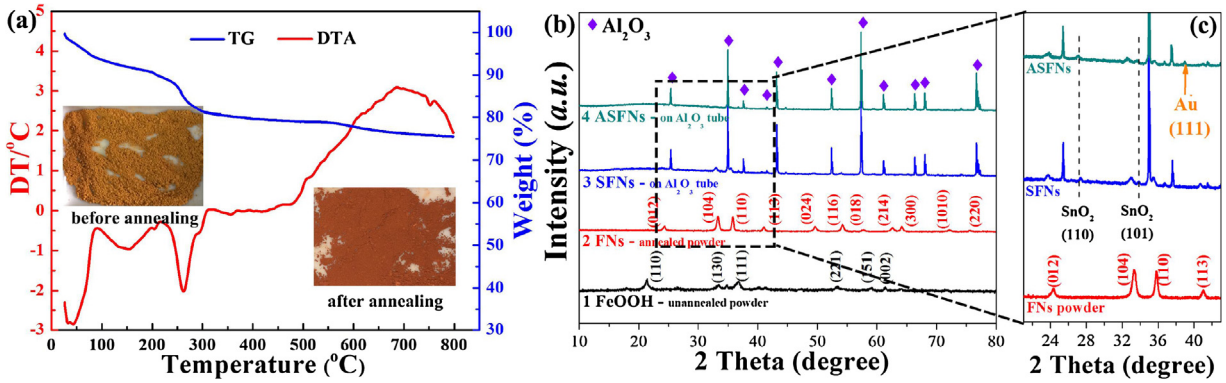

Fig. 1. (a) The TG–DSC curves of precursor samples; (b) the XRD spectra of four kinds of samples in the range of 10°–80°; (c) the XRD spectra of three kinds of samples in the range of 21°–43°.

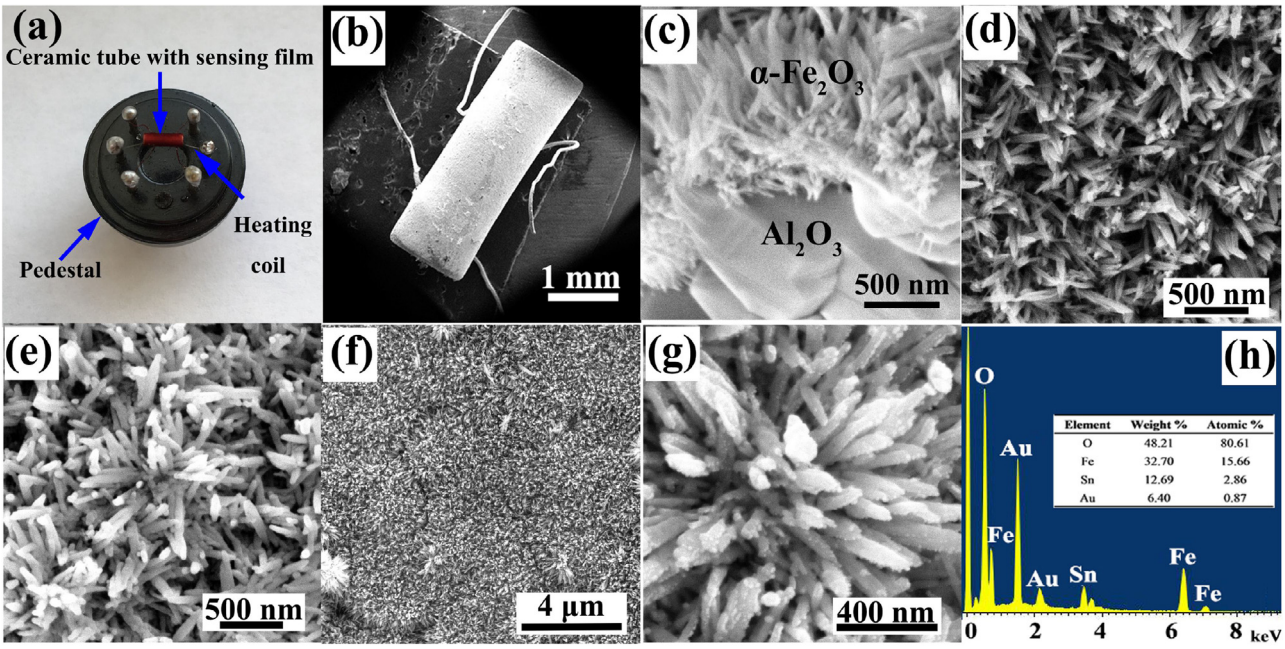

Fig. 2. (a) Gas sensor of α-Fe_2O_3 nanosheets fixed on an electronic bracket (b) Al_2O_3 cube covered with a film of sensing materials; (c) SEM image of SnO_2 nanosheet in cross-sectional view; (d) SEM image of FNs directly grown on Al_2O_3 tubes; (e) SEM images of SFNs; (f, g) SEM images of ASFNS after implantation of SnO_2 shell and Au nanoparitricles; (h) EDS spectrum of ASFNs.

Both diffraction patterns of SFNs sample and ASFNs sample are observed together with the diffraction peaks of Al_2O_3 substrates. Due to the small amount, the XRD peaks of Au and SnO_2 could not be clearly seen when they were deposited onto α-Fe_2O_3 nanoneedles [36].

The sample morphology was characterized by SEM as shown in Fig. 2. Pattern (a) is the SEM image of an Al_2O_3 tube which covered with a film of sensing materials. Fig. 2(b) exhibits the SEM image of FNs which densely grown on the surface of the Al_2O_3 tube. It can be seen that the needles have uniform and homogenous morphologies with about 80 nm in diameter and about 500 nm in length. The SEM image of SFNs is shown in Fig. 2(c), comparing to Fig. 2(a), the diameters of SFNs get lager to 100 nm. Panels (d) and (e) of Fig. 2 are the SEM images of ASFNs in low-magnification and high-magnification, respectively. Some Au particles can be clearly observed on the needles from Fig. 2(e). Pattern (f) of Fig. 2 is the EDS image of ASFNs and no peaks are observed for other impurities. Not only the peaks of O and Fe elements, but those of Au and Sn can also be clearly observed. Moreover, the relative weight and relative atomic of four kinds of elements were listed in the table which was inserted in the graph.

In order to gain further insight into the crystallographic features of the FNs and ASFNs, TEM and associated electron diffraction techniques were employed just as shown in Fig. 3(a–b). The HRTEM analysis of a single FNs reveals a lattice with an interspacing of 0.26 nm, which corresponds to the (104) plane of the α-Fe_2O_3. And the SAED pattern confirms its single-crystalline nature. Similar TEM and HRTEM analyses were also conducted on ASFNs. A single needle with a core-shell configuration of Fe_2O_3 and SnO_2 and many small Au nanoparticles on its surface is shown in Fig. 3(b). The inset pattern shows the corresponding HRTEM image, where the lattice spacing are 0.24 nm of SnO_2 (200) plane and 0.24 nm of Au (111) plane, respectively. The surface composition and structure of the as-synthesized ASFNs were investigated by XPS. The Fig. 3(c) is the XPS full survey spectrum which the peaks of Fe, Sn, Au, O, and C elements can be observed clearly. The presence of C and N element might come from hydrocarbons and nitrogen compounds in the synthesis [36]. Fig. 3(d) displays the high resolution Fe^{3+} 2P spectra of this sample. Both Fe^{3+} $2P_{3/2}$ and Fe^{3+} $2P_{1/2}$ peaks are found to be asymmetric. Panels (e) and (f) of Fig. 3 display the high-resolution spectra for Sn and Au elements, respectively. The peaks of Fig. 3(e) are centered at 487.1and 495.5 eV, which are attributed to the Sn $3d_{5/2}$ and Sn $3d_{3/2}$. The Fig. 3(f) shows the high-resolution Au 4F spectrum of ASFNs. It shows a double feature with peaks located at 83.9 and 87.7 eV, which correspond to the $4f_{7/2}$ and $4f_{5/2}$ signals of metallic Au (Au^0), respectively.

Therefore, combining the analysis of TG-DTA, XRD, SEM, TEM, HRTEM, SAED, and XPS, it can be conclude that an Au-loaded SnO_2 shell coated on the surface of the FNs has been successfully prepared.

3.2. Sensing performance of three kinds of sensors

The Fig. 4(a) presents the relationship of sensing response and the operating temperature. The operating temperature has a very important relationship with the sensing response, which could affect the adsorption and desorption rates of the oxygen species on the metal-oxide surface. The low operating temperature could increase the chemical activation of materials and leading to a relative small response. However, if the operating temperature is too high, the surfeit energies could release the adsorbed gas molecules form the surface of materials before reaction, thus the response will decrease as well [38,39]. Only at the optimum operating temperature, the sensors would have the highest response. As can be seen from the picture, the optimum operating temperature for all three kinds of sensors are is 300 °C. And at 300 °C, to 100 ppm of TEA, the responses of three sensors are 26 (FNs-based sensor), 33 (SFNs-based sensor), and 39 (ASFNs-based sensor), respectively. This performance illustrates that the dopant of Au and composite of SnO_2 played an important role in enhancing the sensing performance. Then, the response decreases as the temperature further increases, which is due to the competing desorption of the chemisorbed oxygen. Besides, the three kinds of sensors have been cycle up to five times and good reversibility can be observed from Fig. 4(b). The experiment was carried out in 100 ppm of TEA at 300 °C. It can be noted that all of the sensors are in good

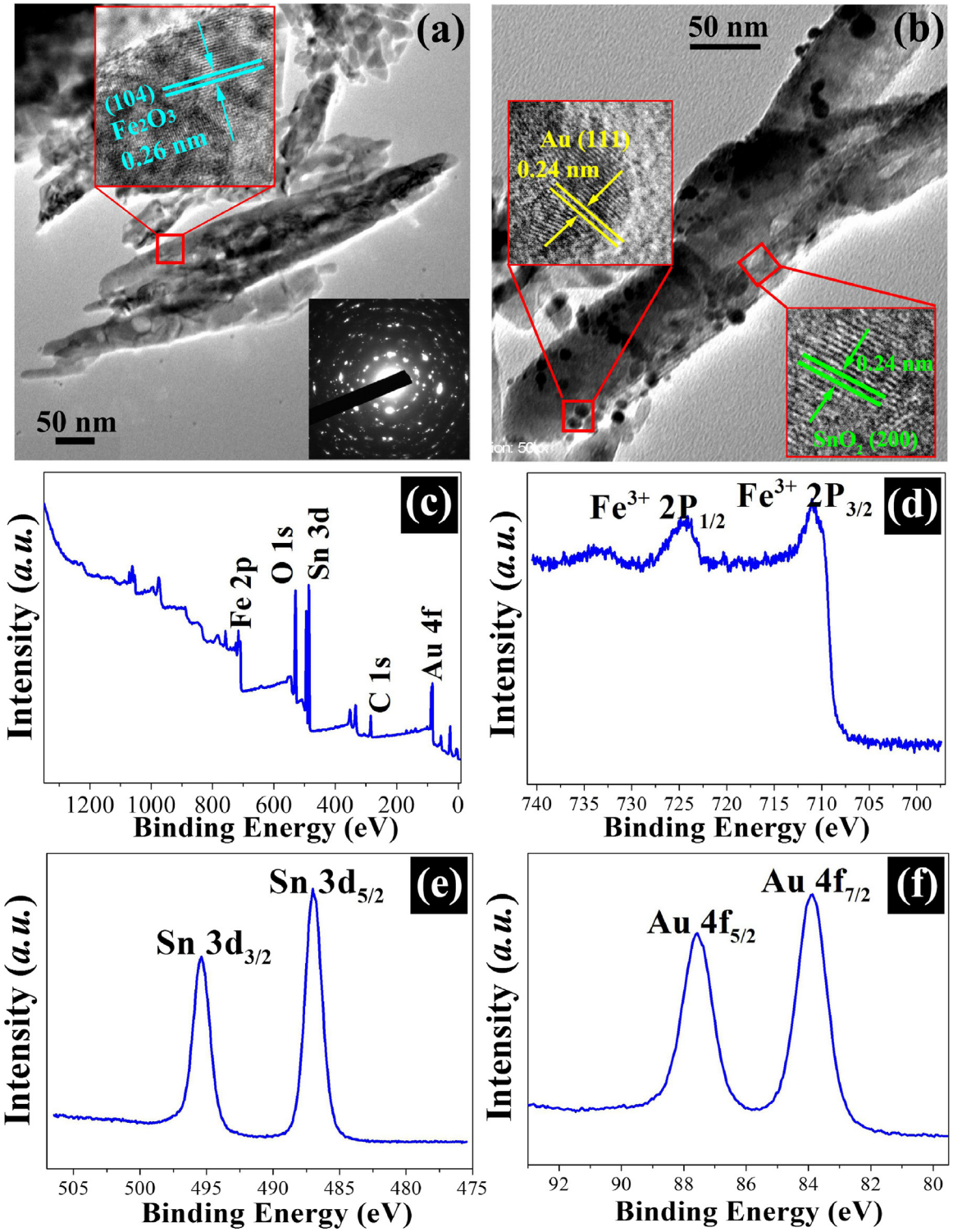

Fig. 3. (a) The TEM, HRTEM, and SAED images of FNs; (b) the TEM and HRTEM images of ASFNs; XPS spectra of the as-synthesized ASFNs: (c) XPS full survey spectrum, (d) Fe 2p spectrum, (e) Sn 3d spectrum, and (f) Au 4f spectrum.

reproducible run after five cycles, which demonstrate a better repeatability of the sensors.

Good selectivity is one of the important criterions of the gas sensors. From Fig. 5, at same concentration of 100 ppm, the response of three kinds of sensor was higher to TEA than other gases such as acetone, ethanol, isopropanol, paraxylene, and benzene at 300 °C. This means that all of the sensors processed a good selectivity to TEA. As expected, the response of ASFNs-based sensor has been enhanced comparing with the other two sensors. Moreover, the response of ASFNs to TEA is much higher than that of the FNs, and it also higher than those interfering gases, indicating an impressive selectivity to TEA. Although the physical reason is still not very clear for us, enhanced selectivity for TEA was observed for ASFNs sensors. One possible reason may be the different reaction activity of target gases in terms of bond energy. The main bond of TEA is C—N with 307 kJ/mol of bond energy, which is relative lower than that

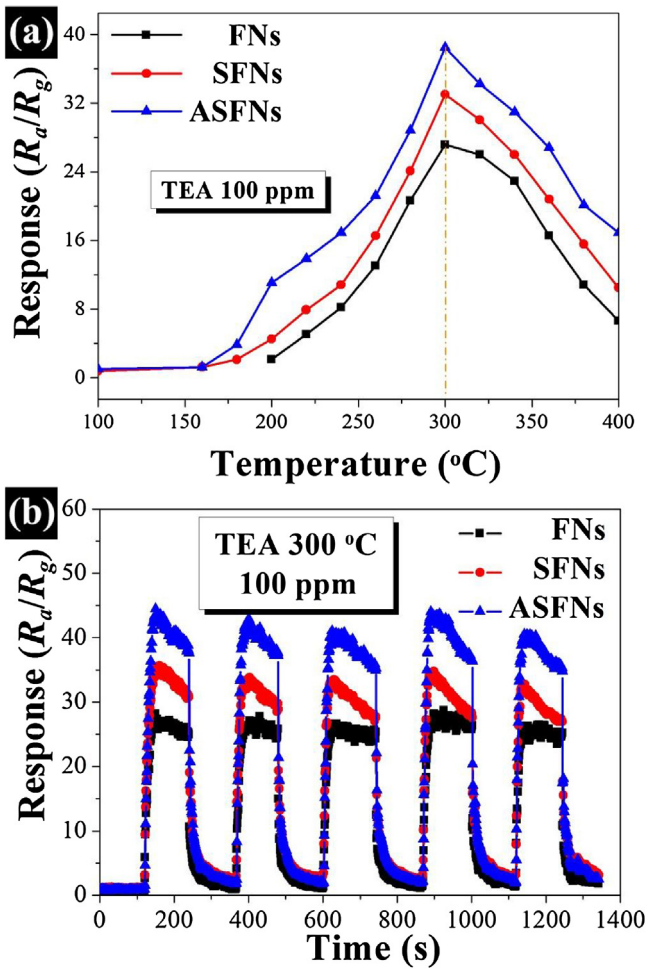

Fig. 4. (a) The relationship between working temperature and response of three kinds of sensors to 100 ppm TEA; (b) the repeatability test of the sensors to 100 ppm TEA at 300 °C.

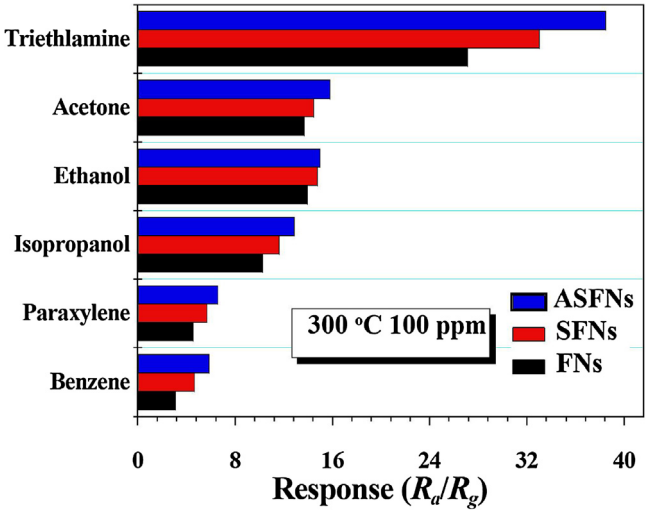

Fig. 5. The selectivity of different gases with same concentration at 300 °C.

of the other gases, such as C—C (345 kJ/mol) of isopropanol, O—H (458.8 kJ/mol) of ethanol, C=C (610.3 kJ/mol) of benzene, and C=O (798.9 kJ/mol) of acetone [40]. So due to the low C—N bond energy, the high reaction activity of TEA molecules would contribute to a high response of Au@SnO_2/α-Fe_2O_3 sensors.

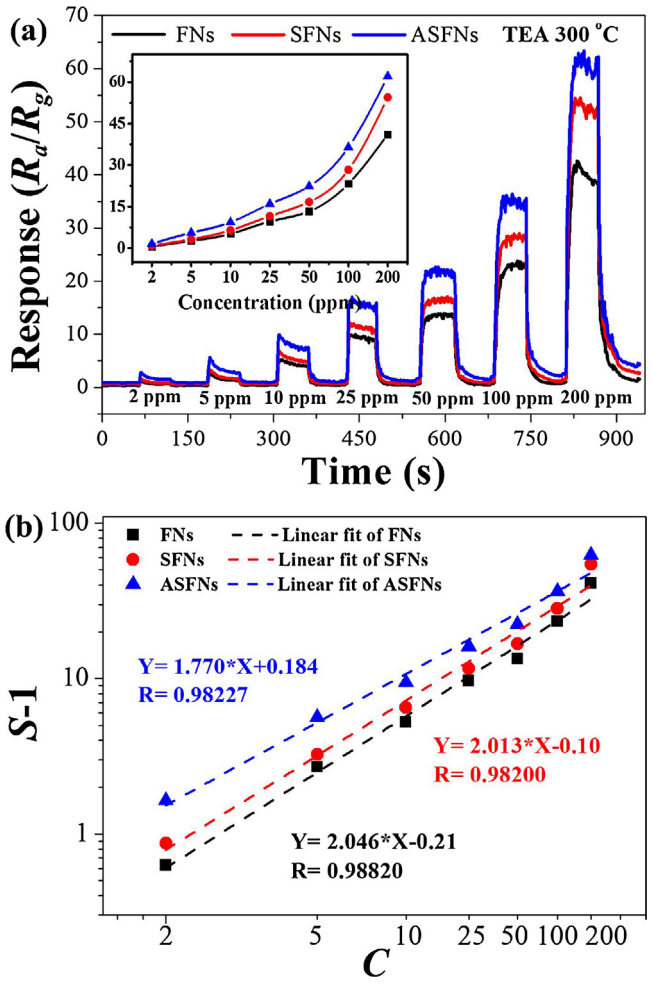

Fig. 6. (a) Response and recovery curves of three kinds of sensors to TEA gas of different concentrations at 300 °C (inset graph) corresponding relationship between sensors response and TEA concentration; (b) the response dilogarithm of three kinds of sensors to the different concentration of TEA.

The relationship of response and concentration has been also studied and shown in Fig. 6. As expected, the response has a positive relationship with increasing TEA concentration from 2 to 200 ppm (Fig. 6(a)). When toward 200 ppm of TEA, the response of ASFNs sensors can reach to 63 which higher than that of the other two kind of sensors. And a relative high response can also be observed upon exposure to the TEA concentration as low as 10 ppm with a better response about 15, which indicate the relatively low detection limit. The relationship of response and concentration would be produced more clearly and intuitive in the inset pattern. Alone with the increasing concentration, the differences between the responses value of the three kinds of sensors are gradually increasing. Fig. 6(b) shows the chart of the response of the sensors (S-1) versus the logarithm of TEA concentration (C). It can be found that the response of the sensor was enhanced linearly with the increase of TEA concentration, indicating a good linearity of sensing characteristics. It is worth noting that the ASFNs sensor fabricated in our work exhibits the best linear property (R = 0.9975) among them. The experiment data were fitted as follows:

$$Y = A + BX$$

Where Y is log (S-1) and X is log (C). A is the value of intercept. B is the value of slope. This result is very attractive for trace TEA detection.

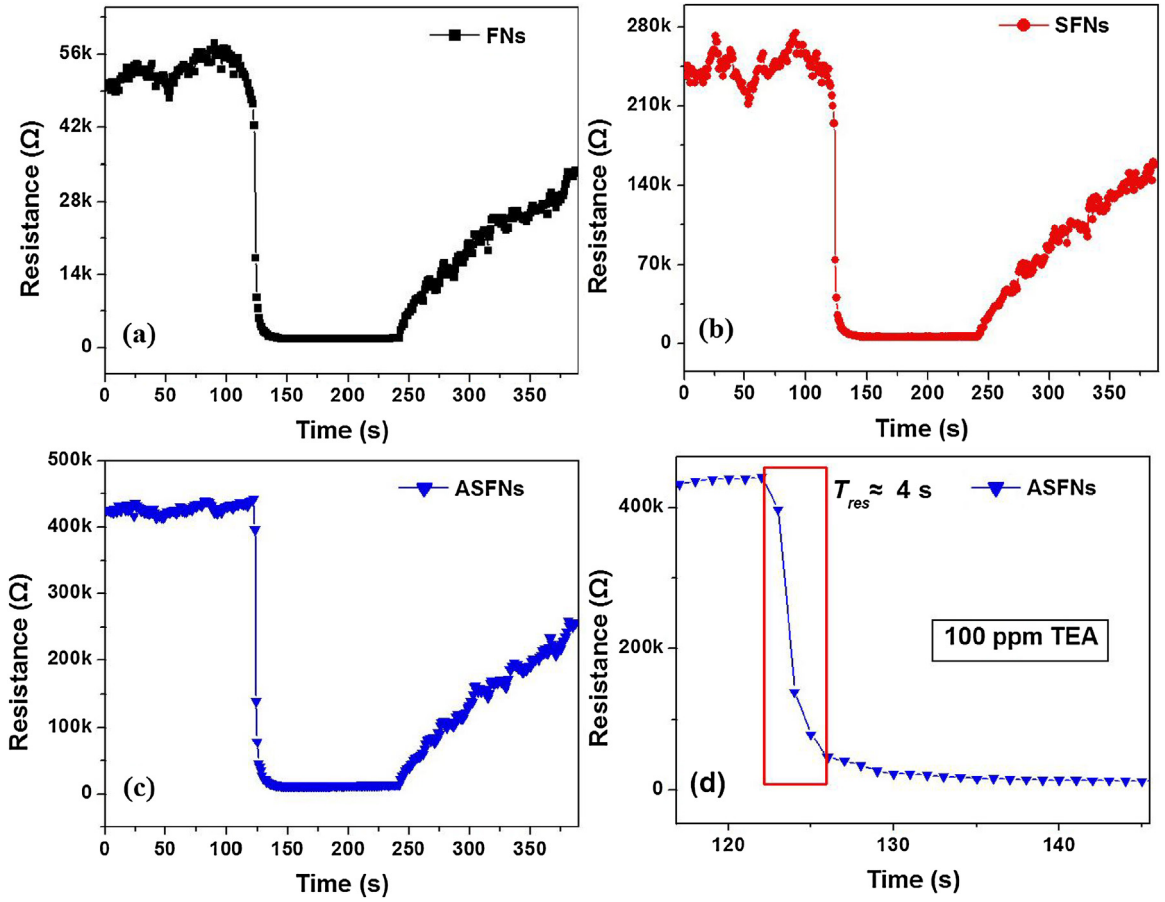

Fig. 7. Response/recovery times of the α-Fe_2O_3 sensors to 100 ppm TEA at 300 °C: (a) pristine α-Fe_2O_3 sensor, (b) SnO_2/α-Fe_2O_3 sensor, and (c) Au@SnO_2/α-Fe_2O_3 sensor; (d) response time of Au@SnO_2/α-Fe_2O_3 sensor taken from (c). The device resistivity at the beginning of measurement (time = 0 s) is the original sensor resistivity in air.

Response and recovery times are also important parameters of gas sensors and real-time detection. The response times (T_{res}) and recovery times (T_{rec}) of a gas sensor are usually defined as the time takes for the resistance to reach 90% of its steady-state value after introduction or removal of the gas, respectively [6,41]. As shown in Fig. 7, when the target gas was injected into the box, all of the three sensors response fast and their response time is 4–9 s, respectively. After desorption, all three kinds of sensors take a long time to recover to the low voltage state.

In summary, the sensing performances of α-Fe_2O_3 sensors have been enhanced by depositing SnO_2 and Au nanoparticles. In order to illustrate the advantages of the sensors, a comparison between the sensing properties of Au@SnO_2/α-Fe_2O_3 sensors and some reported TEA gas sensors is summarized in Table 1 [42,43,40,44–46] in terms of working temperature, response, and response-recovery time. A series of control experimental data on pristine SnO_2, ZnO, MoS_2, α-Fe_2O_3, and TiO_2/SnO_2 sensors are also presented. As we can see that, the Au@SnO_2/α-Fe_2O_3 sensor exhibits short response time, and relatively high response.

3.3. Mechanism discussion of the enhanced sensing properties

The gas sensing response is a very complicated process, whose final mechanism is still unclear. When oxide metal and noble metal are deposited on the surface of pristine semiconductors, the N–N heterojunction and Schottky contact will be formed. As we know, these nanostructures could enhance the sensing performances. However, these leads to a more complex process of gas sensing response. Therefore, it is necessary to study the sensing mechanism of pristine and composited α-Fe_2O_3 sensors, which will be instructive for future work.

First of all, as for n-type semiconductor sensors, the depletion layer model has been well accepted to explain the sensing mechanism [17,47,48]. The resistance of sensors could be effectively changed by the adsorption and desorption of target gas molecules on the surface of sensing materials. This is the basic working principle of the pristine α-Fe_2O_3 sensors. When the α-Fe_2O_3 materials are exposed to fresh air at a relative high temperature, surrounding oxygen molecules will be adsorbed on the surface of crystallites and extract electrons to form oxygen ions species ($O^{\delta-}$: O_2^-, O^{2-}, or O^-). As a result, depletion layers with a certain thickness would appear in the near surface area of crystallites [49]. And the formation of the depletion layer decreases the carrier concentration in the materials and leads to a high resistance of the sensors. We named the resistance in the air as R_{air}. When the materials are exposed to the TEA gas molecules, the gas would be oxidized by negatively charged oxygen ions. The reaction between the TEA gas molecules and $O^{\delta-}$ can be described as follows [46]:

$$(C_2H_5)_3N + O^{\delta-} = CO_2 + H_2O + NO_2 + e^-$$

After reaction, a lot of free electrons are released back into the semiconductor materials. As a result, the thickness of the depletion layer becomes thinner, which decreases the resistance of semiconductor materials that we named R_{gas}. The sensitivity of the sensors is calculated based on the formula of response ($S = R_{air}/R_{gas}$).

Compared with pristine α-Fe_2O_3, the binary SnO_2/α-Fe_2O_3 sensors exhibit enhanced sensing properties, which owing to the formation of N–N heterojunction between two kinds of semicon-

Table 1
TEA sensing performances of as-prepared sensors in our work and other reported sensors, including concentration (Con.), working temperature (W.T.), sensing response (S.R.), and response/recovery time (Res./Rec. Time).

Materials	Con. (ppm)	W.T. (°C)	S.R. (R_a/R_g)	Res./Rec. Time (s)	Ref.
SnO_2 nanorods	1000	350	200	10/10	[42]
ZnO nanorods	50	300	43	10/48	[43]
TiO_2/SnO_2 nanosheets	50	260	26	12/22	[40]
α- Fe_2O_3 microrod	500	275	41	25/55	[44]
SnO_2 flowerlike	100	350	4	<6/6	[45]
MoS_2 nanoflowers	100	300	32	14/114	[46]
α-Fe_2O_3 nanoneedles	100	300	27	6/180	Our work
Au@SnO_2/α-Fe_2O_3 nanoneedles	100	300	39	4/203	

ductors. The schematic model for the sensor exposed to TEA gas with the corresponding change of energy band diagram was shown in Fig. 8. Referring to reports, the work functions of Fe_2O_3 and SnO_2 are 5.88 and 4.9, respectively [50,51]. When the SnO_2 particles are coated onto the surface of the α-Fe_2O_3 nanoneedles, the N–N heterojunction will be formed between SnO_2 and α-Fe_2O_3. This leads to the electrons flowing from SnO_2 to Fe_2O_3 until their Fermi levels equalize. As a result, the energy band would get further bend and an electron depletion layer is created on the surface of SnO_2, which increases the resistance state of sensing materials than that of the pristine α-Fe_2O_3 sensors.

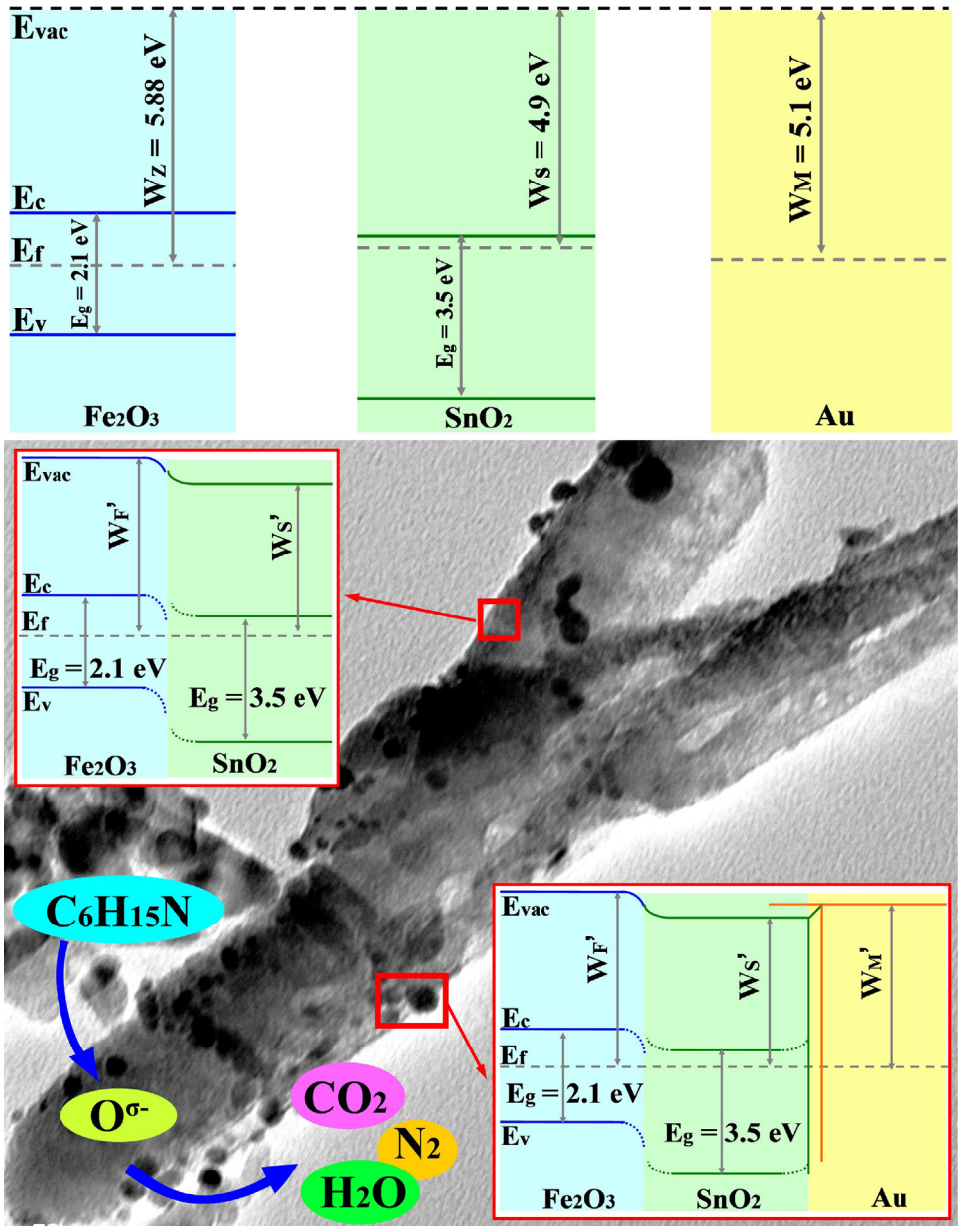

Fig. 8. The schematic model for the sensor exposed to TEA gas with the corresponding change of energy band diagram.

Furthermore, the resistance of sensing materials would be further promoted by building the ternary Au@SnO_2/α-Fe_2O_3 nanostructures. When Au nanoparticles are loaded on the surface of SFNs with core-shell structure, electrons would flow further from SnO_2 to Au, which would form Au-SnO_2 Schottky contact and further widen the depletion layer on the SnO_2 shell. This leads to further increasing the resistance of the ASFNs sensors which means a higher sensing response. The energy band diagram of the above two kinds of conditions is shown in the inset of Fig. 8. Therefore, when the Au@SnO_2/α-Fe_2O_3 composite sensing materials are exposed to the reducing TEA gas, the width of the depletion layer will be reduced more significantly than that of pristine α-Fe_2O_3, resulting in a great decrease of resistance.

In other words, the increase of initial resistance should be one of mainly reasons for the enhancement of gas sensing properties. The change of material resistance could be directly observed in Fig. 7. In air, the resistance of pristine α-Fe_2O_3 is nearly 50 kΩ. After deposited with SnO_2 nanoparticles, its resistance increased to nearly 245 kΩ. It is worth noting that the resistance of Au@SnO_2/α-Fe_2O_3 could reach up to nearly 430 kΩ. When the three kinds of sensors get stable in the TEA vapor, the electrons are released back to the conduction band of material. Then, the resistance of three kinds of sensors becomes similar as a result. On the basis of definition of sensing response ($S = R_a/R_g$), the values of sensitivity could be calculated. That is to say, the enhanced response to TEA is mainly attributed to the variation of resistance caused by the formation of the N–N heterojunction and Au-SnO_2 Schottky barrier. This result illustrates that the design of composite sensing materials is very effective to improve sensor performances affectively.

4. Conclusions

In this manuscript, we reported a highly sensitive and selective TEA sensor by the formation of SnO_2/Fe_2O_3 N–N heterostructure and Au-SnO_2 Schottky contact and the enhanced gas sensing mechanism was discussed in detail. The α-Fe_2O_3 nanoneedles were directly grown on Al_2O_3 tubes by a simple and environment-friendly hydrothermal method. Then, the Au@SnO_2/α-Fe_2O_3 nanostructure is built by PLD and DC-Sputtering method. In comparison with the sensing properties of pristine α-Fe_2O_3 sensor, the Au@SnO_2/α-Fe_2O_3 composite nanostructures exhibit higher sensing response and better linearity. The N–N heterojunction and Schottky contact formed in the Au@SnO_2/α-Fe_2O_3 sensor obviously increases the resistance in air and decreases the resistance in the TEA gas. This is the main reason for the enhanced response to TEA. This study presents an effective way to design and fabricate chemiresistance gas sensors with high performance.

Acknowledgements

This work is supported by Shandong Provincial Key Research and Development Program (No. 2017GGX10135), Shandong Provincial Science Foundation (No. ZR2014JL045).

Appendix A. Supplementary data

Supplementary data associated with this article can be found, in the online version, at https://doi.org/10.1016/j.snb.2018.01.209.

References

[1] X. Liu, S. Cheng, H. Liu, S. Hu, D. Zhang, H. Ning, A survey on gas sensing technology, Sensors 12 (2012) 9635–9665.
[2] K.J. Huang, J.Z. Zhang, Y.J. Liu, L.L. Wang, Novel electrochemical sensing platform based on molybdenum disulfide nanosheets-polyaniline composites and Au nanoparticles, Sens. Actuators B 194 (2014) 303–310.
[3] M. Peris, L. Escuder-Gilabert, A 21st century technique for food control: electronic noses, Anal. Chim. Acta 638 (2009) 1–15.
[4] C. Sapsanis, H. Omran, V. Chernikova, O. Shekhah, Y. Belmabkhout, U. Buttner, M. Eddaoudi, K.N. Salama, Insights on capacitive interdigitated electrodes coated with MOF thin films: humidity and VOCs sensing as a case study, Sensors 15 (2015) 18153–18166.
[5] T. Zhai, H.Y. Xu, W.R. Li, H.Q. Yu, Z.R. Chen, J.Q. Wang, B.Q. Cao, Low-temperature in-situ growth of SnO_2 nanosheets and its high triethylamine sensing response by constructing Au-loaded ZnO/SnO_2 heterostructure, J. Alloy. Compd. 737 (2018) 603–612.
[6] D.X. Ju, H.Y. Xu, Q. Xu, H.B. Gong, Z.W. Qiu, J. Guo, J. Zhang, B.Q. Cao, High triethylamine-sensing properties of NiO/SnO_2 hollow sphere P-N heterojunction sensors, Sens. Actuators B 215 (2015) 39–44.
[7] B. Gandu, K. Sandhya, A.G. Rao, Y.V. Swamy, Gas phase bio-filter for the removal of triethylamine (TEA) from air: microbial diversity analysis with reference to design parameters, Bioresour. Technol. 139 (2013) 155–160.
[8] P. Sun, X.D. Mei, Y.X. Cai, J. Ma, Y.F. Sun, X.S. Liang, F.M. Liu, G.Y. Lu, Synthesis and gas sensing properties of hierarchical SnO_2 nanostructures, Sens. Actuators B 187 (2013) 301–307.
[9] S.M. Wang, B.X. Xiao, T.Y. Yang, P. Wang, C.H. Xiao, Z.F. Li, R. Zhao, M.Z. Zhang, Enhanced HCHO gas sensing properties by Ag-loaded sunflower-like In_2O_3 hierarchical nanostructures, J. Mater. Chem. A 2 (2014) 6598–6604.
[10] H.D. Zheng, J.Z. Ou, M.S. Strano, R.B. Kaner, A. Mitchell, K. Kalantar-zadeh, Nanostructured tungsten oxide-properties, synthesis, and applications, Adv. Funct. Mater. 21 (2011) 2175–2196.
[11] M.H. Seo, M. Yuasa, T. Kid, J.S. Huh, N. Yamazoe, K. Shimanoe, Microstructure control of TiO_2 nanotubular films for improved VOC sensing, Sens. Actuators B 154 (2011) 251–256.
[12] G.X. Zhu, H. Xu, Y.Y. Xiao, Y.J. Liu, A.H. Yuan, X.P. Shen, Facile fabrication and enhanced sensing properties of hierarchically porous CuO architectures, ACS Appl. Mater. Interfaces 4 (2012) 744–751.
[13] C.C. Li, X.M. Yin, T.H. Wang, H.C. Zeng, Morphogenesis of highly uniform $CoCO_3$ submicrometer crystals and their conversation to mesoporous Co_3O_4 for gas-sensing applications, Chem. Mater. 21 (2009) 4984–4992.
[14] H. Huang, H. Gong, C.L. Chow, J. Guo, T.J. White, M.S. Tse, O.K. Tan, Low-temperature growth of SnO_2 nanorod arrays and tunable n-p-n sensing response of a ZnO/SnO_2 heterojunction for exclusive hydrogen sensors, Adv. Funct. Mater. 21 (2011) 2680–2686.
[15] A. Das, V. Bonu, A.K. Prasad, D. Panda, S. Dharaa, A.K. Tyagi, The role of SnO_2 quantum dots in improved CH_4 sensing at low temperature, J. Mater. Chem. C 2 (2014) 164–171.
[16] S.L. Bai, K.W. Zhang, R.X. Luo, D.Q. Li, A.F. Chen, C.C. Liu, Low-temperature hydrothermal synthesis of WO_3 nanorods and their sensing properties for NO_2, J. Mater. Chem. 22 (2012) 12643–12650.
[17] Z.J. Li, Y.W. Huang, S.C. Zhang, W.M. Chen, Z. Kuang, D.Y. Ao, W. Liu, Y.Q. Fu, A fast response & recovery H_2S gas sensor based on α-Fe_2O_3 nanoparticles with ppb level detection limit, J. Hazard. Mater. 300 (2015) 167–174.
[18] Z.J. Li, W.Z. Shen, W.S. He, X.T. Zu, Effect of Fe-doped TiO_2 nanoparticle derived from modified hydrothermal process on the photocatalytic degradation performance on methylene blue, J. Hazard. Mater. 155 (2008) 590–594.
[19] L. Yue, K.H. Wang, J.B. Guo, J.L. Yang, X. Luo, J. Lian, L. Wang, Enhance delectrochemical oxidation of dye waste water with Fe_2O_3 supported catalyst, J. Ind. Eng. Chem. 20 (2014) 725–731.
[20] H. Katsuki, S. Komarneni, Role of α-Fe_2O_3 morphology on the color of redpigment for porcelain, J. Am. Ceram. Soc. 86 (2003) 183–185.
[21] J.T. Wu, S.Y. Mao, Z.G. Ye, Z.X. Xie, L.S. Zheng, Room-temperature weak ferromagnetism induced by point defects in alpha-Fe_2O_3, Appl. Mater. Interfaces 2 (2010) 1561–1564.
[22] M.H. Chen, J.L. Liu, D.L. Chao, J. Wang, J.H. Yin, J.Y. Lin, H.J. Fan, Z.X. Shen, Porous alpha-Fe_2O_3 nanorods supported on carbon nanotubes-graphene foam as superior anode for lithium ion batteries, Nano Energy 9 (2014) 364–372.
[23] Y.W. Huang, W.M. Chen, Z.C. Zhang, Z. Kuang, D.Y. Ao, N.R. Alkurd, W.L. Zhou, W. Liu, W.Z. Shen, Z.J. Li, A high performance hydrogen sulfide gas sensor based on porous α-Fe_2O_3 operates at room-temperature, Appl. Surf. Sci. 351 (2015) 1025–1033.
[24] D.P. Volanti, A.A. Felix, M.O. Orlandi, G. Whitfield, D. Yang, E. Longo, H.L. Tuller, J.A. Varela, The role of hierarchical morphologies in the superior gas sensing performance of CuO-based chemiresistors, Adv. Funct. Mater. 23 (2013) 1759–1766.
[25] H. Wang, K. Dou, W.Y. Teoh, Y. Zhan, T. Hung, F. Zhang, J. Xu, R. Zhang, A.L. Rogach, Engineering of facets band structure, and gas-sensing properties of hierarchical Sn^{2+}-doped SnO_2 nanostructures, Adv. Funct. Mater. 23 (2013) 4847–4853.
[26] D. Chen, L. Ge, L. Yin, H. Shi, D. Yang, J. Yang, R. Zhang, G.S. Shao, Solvent-regulated solvothermal synthesis and morphology-dependent gas-sensing performance of low-dimensional tungsten oxide nanocrystals, Sens. Actuators B 205 (2014) 391–400.
[27] C. Sun, X. Su, F. Xiao, C. Niu, J. Wang, Synthesis of nearly monodisperse Co_3O_4 nanocubes via a microwave-assisted solvothermal process and their gas sensing properties, Sens. Actuators B 157 (2011) 681–685.
[28] Y.H. Choi, D.H. Kim, H.S. Han, S. Shin, S.H. Hong, K.S. Hong, Direct printing synthesis of self-organized copper oxide hollow spheres on a substrate using copper(II) complex ink: gas sensing and photoelectro chemical properties, Langmuir 30 (2014) 700–709.
[29] T. Ishikawa, E. Matijevic, Formation of monodispersed pure and coated spindle-type iron particles, Langmuir 4 (1988) 26–31.

[30] Y. Wang, J.L. Cao, S.R. Wang, X.Z. Guo, J. Zhang, H.J. Xia, S.M. Zhang, S.H. Wu, Facile synthesis of porous α-Fe_2O_3 nanorods and their application in ethanol sensors, J. Phys. Chem. C 112 (2008) 17804–17808.
[31] G. Wang, X. Gou, J. Horvat, J. Park, Facile synthesis and characterization of iron oxide semiconductor nanowires for gas sensing application, J. Phys. Chem. C 112 (2008) 15220–15225.
[32] Z. Chen, U. Cvelbar, M. Mozetic, J. He, M.K. Sunkara, Long-range ordering of oxygen-vacancy planes in α-Fe_2O_3 nanowires and nanobelts, Chem. Mater. 20 (2008) 3224–3228.
[33] C.J. Jia, L.D. Sun, Z.G. Yan, L.P. You, F. Luo, X.D. Han, Y.C. Pang, Z. Zhang, C.H. Yan, Single-crystalline iron oxide nanotubes, Angew. Chem. 117 (2005) 4402–4407.
[34] S.L. Zhong, J.M. Song, S. Zhang, H. Yao, A.W. Xu, W.T. Yao, S.H. Yu, Template-free hydrothermal synthesis and formation mechanism of hematite microrings, J. Phys. Chem. C 112 (2008) 19916–19921.
[35] X. Gou, G. Wang, J. Park, H. Liu, J. Yang, Monodisperse hematite porous nanospheres: synthesis, characterization, and applications for gas sensors, Nanotechnology 19 (2008) 1–7.
[36] D.X. Ju, H.Y. Xu, Z.W. Qiu, Z.C. Zhang, Q. Xu, J. Zhang, J.Q. Wang, B.Q. Cao, Near room temperature fast-response, and highly sensitive triethylamine sensor assembled with Au-loaded ZnO/SnO_2 core–shell nanorods on flat alumina substrates, ACS Appl. Mater. Interfaces 7 (2015) 19163–19171.
[37] Y.E. Mendili, J.F. Bardeau, N. Randrianantoandro, F. Grasset, J.M. Greneche, Insights into the mechanism related to the phase transition from γ-Fe_2O_3 to α-Fe_2O_3 nanoparticles induced by thermal treatment and laser irradiation, J. Phys. Chem. C 116 (2012) 23785–23792.
[38] C.W. Zou, J. Wang, W. Xie, Synthesis and enhanced NO_2 gas sensing properties of ZnO nanorods/TiO_2 nanoparticles heterojunction composites, J. Colloid Interface Sci. 478 (2016) 22–28.
[39] L.J. Bie, X.N. Yan, J. Yin, Y.Q. Duan, Z.H. Yuan, Nanopillar ZnO gas sensor for hydrogen and ethanol, Sens. Actuators B 126 (2007) 604–608.
[40] H.Y. Xu, D.X. Ju, W.R. Li, J. Zhang, J.Q. Wang, B.Q. Cao, Superior triethylamine-sensing properties based on TiO_2/SnO_2 n–n heterojunction nanosheets directly grown on ceramic tubes, Sens. Actuators B 228 (2016) 634–642.
[41] Y.J. Xie, J.P. Du, R.H. Zhao, H.Y. Wang, H.L. Yao, Facile synthesis of hexagonalbrick-shaped SnO_2 and its gas sensing toward triethylamine, J. Environ. Chem. Eng. 1 (2013) 1380–1384.
[42] D. Wang, X.F. Chu, M.L. Gong, Gas sensing properties of sensors based on single-crystalline SnO_2 nanorods prepared by a simple molten-salt method, Sens. Actuators B 117 (2006) 183–187.
[43] W.R. Li, H.Y. Xu, T. Zhai, H.Q. Yu, Q. Xu, X.P. Song, J.Q. Wang, B.Q. Cao, High-sensitivity high-selectivity, and fast-recovery-speed triethylamine sensor based on ZnO micropyramids prepared by molten salt growth method, J. Alloys Compd. 695 (2017) 2930–2936.
[44] G. Sun, H.L. Chen, Y.W. Li, G.Z. Ma, S.S. Zhang, T.K. Jia, J.L. Cao, X.D. Wang, H. Bala, Z.Y. Zhang, Synthesis and triethylamine sensing properties of mesoporous α-Fe_2O_3 microrods, Mater. Lett. 178 (2016) 213–216.
[45] X.F. Chu, D.L. Jiang, C.M. Zheng, The preparation and gas sensing properties of $NiFe_2O_4$ nanocubes and nanorods, Sens. Actuators B 123 (2007) 793–797.
[46] W.R. Li, H.Y. Xu, T. Zhai, H.Q. Yu, Z.W. Qiu, X.P. Song, J.Q. Wang, B.Q. Cao, Enhanced triethylamine sensing properties by designing Au@SnO_2/MoS_2 nanostructure directly on alumina tubes, Sens. Actuators B 253 (2017) 97–107.
[47] H.Y. Xu, D.X. Ju, W.R. Li, H.B. Gong, J. Zhang, J.Q. Wang, B.Q. Cao, Low-working-temperature, fast-response-speed NO_2 sensor with nanoporous-SnO_2/polyaniline double-layered film, Sens. Actuators B 224 (2016) 654–660.
[48] Z. Lou, F. Li, J.N. Deng, L.L. Wang, T. Zhang, Branch-like hierarchical heterostructure (α-Fe_2O_3/TiO_2): a novel sensing material for trimethylamine gas sensorl, ACS Appl. Mater. Interfaces 5 (2013) 12310–12316.
[49] Y.J. Chen, L. Yu, D.D. Feng, M. Zhuo, M. Zhang, E.D. Zhang, Z. Xu, Q.H. Li, T.H. Wang, Superior ethanol-sensing properties based on Ni-doped SnO_2 p-n heterojunction hollow spheres, Sens. Actuators B 166–167 (2012) 61–67.
[50] M.T. Niu, F. Huang, L.F. Cui, P. Huang, Y.L. Yu, Y.S. Wang, Hydrothermal synthesis, structural characteristics, and enhanced photocatalysis of SnO_2/α-Fe_2O_3 semiconductor nanoheterostructures, ACS Nano 4 (2010) 681–688.
[51] B. Mondala, B. Basumatari, J. Dasb, C. Roychaudhury, H. Saha, N. Mukherjee, ZnO-SnO_2 based composite type gas sensor for selective hydrogen sensing, Sens. Actuators B 194 (2014) 389–396.

Biographies

Hongyan Xu received her Ph.D. degree from State Key Lab of Crystal Materials, Shandong University in 2006. Now she is an Associate Professor at School of Materials Science and Engineering, University of Jinan. Her main research interests are the synthesis and fabrication of semiconductor nano-materials and high performance conductive polymer composite chemical gas sensors.

Wenru Li graduated from School of Materials Science and Engineering, University of Jinan in 2015. Now he is a graduate student focusing on gas sensing materials for master degree the same university.

Rui Han is currently studying for the B.A. degree in the School of Materials Science and Engineering, University of Jinan, China. Now her research interests focus on the nanostructured semiconductor materials for the gas sensor applications.

Ting Zhai is graduatedfrom School of MaterialsScience and Engineering, University of Jinan in 2016.Now she is a graduate student focusing on gas sensing materials formaster degree the same university.

Huanqin Yu is currently studying for the M.S. degree in theSchool of MaterialsScience and Engineering, University of Jinan, China. Now herresearch interests focus on the nanostructured semiconductor materials for the gas sensor applications.

Zhengrun Chen graduated from School of Materials Science and Engineering, University of Jinan in 2017. Now he is a graduate student focusing on gas sensing materials for master degree the same university.

Xiangwen Wu received her Ph.D. degree from State Key Lab of Crystal Materials, Shandong University in 2003. Now she is an Associate Professor at College of Chemistry, Shandong Normal University. Her main research interests are the synthesis and fabrication of metal-organic frameworks (MOFs) functional materials.

Jieqiang Wang received his Ph.D. degree from Northeastern University in 1999. Now he works as a Professor at School of Materials Science and Engineering, University of Jinan. His researches focus on the synthesis and fabrication of semiconductor nano-materials.

Bingqiang Cao received the Ph.D. degree from the Institute of Solid State Physics, Chinese Academy of Sciences (CAS) in 2006. After that, he worked as a postdoctoral researcher at University of Leipzig from September 2006 to August 2008, and then as a JSPS fellow at Kyushu University from August 2008 to July 2009. Now, he is a Principle Investigator and Oversea Taishan Scholar endowed professor of University of Jinan in China. His research is focused on nanostructures, heterostructures, thin films, and transparent optoelectrical devices based on inorganic semiconductors.